

Non-iterative parameter estimation of the 2R-1C model suitable for low-cost embedded hardware*

Mitar SIMIĆ^{†‡1}, Zdenka BABIĆ¹, Vladimir RISOJEVIĆ¹, Goran M. STOJANOVIĆ²

¹Faculty of Electrical Engineering, University of Banja Luka, Banja Luka 78000, Bosnia and Herzegovina

²Faculty of Technical Sciences, University of Novi Sad, Novi Sad 21000, Republic of Serbia

[†]E-mail: mitar.simic@etf.unibl.org

Received Feb. 26, 2019; Revision accepted June 23, 2019; Crosschecked Sept. 6, 2019; Published online Oct. 29, 2019

Abstract: Parameter estimation of the 2R-1C model is usually performed using iterative methods that require high-performance processing units. Consequently, there is a strong motivation to develop less time-consuming and more power-efficient parameter estimation methods. Such low-complexity algorithms would be suitable for implementation in portable microcontroller-based devices. In this study, we propose the quadratic interpolation non-iterative parameter estimation (QINIFE) method, based on quadratic interpolation of the imaginary part of the measured impedance, which enables more accurate estimation of the characteristic frequency. The 2R-1C model parameters are subsequently calculated from the real and imaginary parts of the measured impedance using a set of closed-form expressions. Comparative analysis conducted on the impedance data of the 2R-1C model obtained in both simulation and measurements shows that the proposed QINIFE method reduces the number of required measurement points by 80% in comparison with our previously reported non-iterative parameter estimation (NIFE) method, while keeping the relative estimation error to less than 1% for all estimated parameters. Both non-iterative methods are implemented on a microcontroller-based device; the estimation accuracy, RAM, flash memory usage, and execution time are monitored. Experiments show that the QINIFE method slightly increases the execution time by 0.576 ms (about 6.7%), and requires 24% (1.2 KB) more flash memory and just 2.4% (32 bytes) more RAM in comparison to the NIFE method. However, the impedance root mean square errors (RMSEs) of the QINIFE method are decreased to 42.8% (for the real part) and 64.5% (for the imaginary part) of the corresponding RMSEs obtained using the NIFE method. Moreover, we compared the QINIFE and the complex nonlinear least squares (CNLS) estimation of the 2R-1C model parameters. The results obtained show that although the estimation accuracy of the QINIFE is somewhat lower than the estimation accuracy of the CNLS, it is still satisfactory for many practical purposes and its execution time reduces to $\frac{1}{45} - \frac{1}{30}$.

Key words: 2R-1C model; Embedded systems; Parameter estimation; Non-iterative methods; Quadratic interpolation

<https://doi.org/10.1631/FITEE.1900112>


CLC number: O231

1 Introduction

Non-destructive techniques for evaluation of the properties of materials, processes, and structures including electrical impedance spectroscopy, dielectric spectroscopy, thermal imaging, eddy current testing, as well as magnetic particle, radiographic, and ultrasonic methods, have been a topic of high importance and interest in the scientific community.

[‡] Corresponding author

* Project supported by the Ministry of Science and Technology of the Republic of Srpska (No. 19/6-020/961-143/18) and the EU's H2020 MSCA MEDLEM (No. 690876)

 ORCID: Mitar SIMIĆ, <http://orcid.org/0000-0002-8300-022X>

© Zhejiang University and Springer-Verlag GmbH Germany, part of Springer Nature 2019

For example, electrical impedance spectroscopy is a powerful and widely used technique in many fields for unraveling the complex nonlinear processes of many material-material interfaces and applications. In these applications, measured electrical impedance as a function of the excitation frequency can reveal the internal dynamics of underlying processes (Barsoukov and Macdonald, 2005). Different material-material interfaces, structural characteristics, and internal connections can be modeled using equivalent electrical circuits. In the literature, electrical circuits have been reported as an approach for modeling of sensors (Simić et al., 2017b; Vargas-Bernal et al., 2018), biological cells and bioimpedance (Qiao et al., 2012; Sánchez Terrones et al., 2013), solar cells (Kern et al., 2002), proton exchange membrane (PEM) fuel cells (Wang et al., 2005), batteries (Moss et al., 2008; Dong et al., 2011), as well as in unsteady heat transfer analysis (Wang et al., 2018) and prediction of total body water volume (Gheorghe et al., 2012).

The structure of an equivalent electrical circuit is usually chosen based on previous knowledge of the structure of the materials, material-material interfaces, and the physical processes involved. Estimation of model parameters focuses on finding their values, thus ensuring a small difference between the measured impedance and the impedance calculated using the estimated values of the model parameters. Equivalent circuit models have traditionally consisted of basic electrical elements such as resistors (R), inductors (L), and capacitors (C). However, the continuously increasing power of available computing units allows the use of very complex models containing empirical elements such as the constant phase element (CPE) and the Warburg diffusion element. Recently, concepts from fractional calculus (i.e., non-integer order differentiation) and integration have also been applied to parameter estimation of equivalent electrical circuits (Maundy et al., 2015; Freeborn et al., 2017; Al-Ali et al., 2018). Nevertheless, many electrochemical processes have inherently capacitive electrical behaviors, which can be modeled using simple R-C models, rather than more complex models (Kern et al., 2002; Wang CS et al., 2005; Moss et al., 2008; Dong et al., 2011; Gheorghe et al., 2012; Qiao et al., 2012; Sánchez Terrones et al., 2013; Manjakkal et al., 2014, 2015a, 2015b; Simić et al., 2017b; Vargas-Bernal et al., 2018; Wang Z et

al., 2018). A notable example is the parallel 2R-1C model, which consists of two resistors (R_1 and R_2) and one capacitor (C_2), with two branches connected in parallel (Fig. 1). Its popularity is mainly due to its simplicity and ability to assign a direct physical interpretation to model parameters (Sanchez et al., 2013).

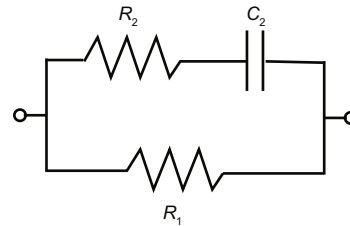


Fig. 1 The parallel 2R-1C model

As an example, in bioimpedance analysis a biological cell can be modeled using the parallel 2R-1C model, where R_1 is the resistance of the extracellular space, R_2 the resistance of the intracellular space, and C_2 represents the capacitance of the cell membrane. Furthermore, the 2R-1C model allows identification of changes in model parameters which represent changes in the corresponding physical phenomena. Specifically, changes in cell membrane capacitance (C_2 in the model) reflect the characteristic features of the occurrence of many processes in the cell (Bertrand and Hopfer, 2002), such as the fusion of vesicles with the plasma membrane (Santos-Sacchi, 2004), particle uptake after cellular exposure to phagocytic stimuli (Holevinsky and Nelson, 1998), or cell temperature changes (Hotka and Zahradnik, 2014). The use of the 2R-1C model in bioimpedance analysis has also been reported in measuring changes in volume within an organ or the whole body (Ferreira et al., 2013), in vivo time-varying human lung tissue characterization (Sanchez et al., 2013), and body water volume estimation (Gheorghe et al., 2012). Finally, the 2R-1C model has been used in commercial bioimpedance spectroscopy devices, such as the ImpediMed SFB7 and Xitron Hydra 4200, which estimate the values of the model parameters starting from the measured bioimpedance.

It is well known that the model of biological tissue impedance using the Cole function shows better results in fitting experimental high-frequency impedance data (Lazović et al., 2014; Yousri et al., 2017). However, instead of capacitor C_2 , the Cole

function contains a CPE element which does not have a clear physical meaning. Consequently, the interpretability of the parameters along with its simplicity makes the 2R-1C model an interesting alternative to the more complex Cole function. Therefore, in this study we decide to restrict our discussion to the 2R-1C model.

A structure similar to the parallel 2R-1C model, formed with a resistor (R'_1) in series with a parallel R-C circuit (R'_2 and C'_2), known as the series 2R-1C model, is shown in Fig. 2.

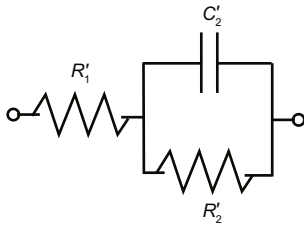


Fig. 2 The series 2R-1C model

However, both 2R-1C models from Figs. 1 and 2 are isospectral if the following conditions are satisfied:

$$R'_1 = \frac{R_1 R_2}{R_1 + R_2}, \quad (1)$$

$$R'_2 = \frac{R_1^2}{R_1 + R_2}, \quad (2)$$

$$C'_2 = \frac{C_2 (R_1 + R_2)^2}{R_1^2}. \quad (3)$$

In the rest of this study we will use the term 2R-1C model for the structure shown in Fig. 1, with a note that complete analysis can be easily transferred to the model from Fig. 2. Furthermore, because the meaning of the 2R-1C model parameters depends on the application of the model, we will consider a general case without discussing the physical interpretation of model parameters.

The complex impedance of the 2R-1C model at some angular frequency ω is given with

$$\begin{aligned} \underline{Z}(\omega) &= R(\omega) + jX(\omega) \\ &= \frac{R_1(1 + j\omega C_2 R_2)}{1 + j\omega C_2 (R_1 + R_2)}, \end{aligned} \quad (4)$$

where $R(\omega)$ and $X(\omega)$ stand for the real (resistance) and imaginary (reactance) parts of $\underline{Z}(\omega)$, respectively.

Because the 2R-1C model consists of three parameters (R_1 , R_2 , and C_2) while just two measured values ($R(\omega)$ and $X(\omega)$) are available at some frequency ω , it is not possible to have a unique analytical solution of such a system of equations. Iterative methods such as the Taylor polynomial (Ortega and Rheinboldt, 1970), the Adomian decomposition method (Babolian et al., 2004; Abbasbandy, 2005; Darvishi and Barati, 2007), the homotopy perturbation method (Golbabai and Javidi, 2007), quadrature formulas (Cordero and Torregrosa, 2007; Noor, 2007), Levenberg-Marquardt, and the trust region algorithms in the nonlinear least squares approach (Bondarenko, 2012; Boinet et al., 2016; Boukamp and Rolle, 2018) have been widely used for such a class of mathematical problems.

However, iterative methods have some limitations regarding time consumption, slow signal processing, possibility of converging towards a local minimum, as well as requiring a high-quality starting point for the values of model parameters (Sanchez et al., 2013). Thus, new methods for parameter estimation of the 2R-1C model are continuously being developed, such as differential impedance analysis (Sanchez et al., 2013; Simić et al., 2017a), the local polynomial method (Sanchez et al., 2011), use of multisine excitations instead of the classical technique of frequency sweep for impedance measurement (Sanchez et al., 2012), and more recently, fast spectral measurements and regularization (Ramírez-Chavarría et al., 2018). However, the approaches described in Sanchez et al. (2011, 2012, 2013) and Ramírez-Chavarría et al. (2018) are not optimized for low-cost systems with low power processing units because they require complex mathematical operations. Therefore, these approaches are typically implemented on PC-based platforms.

The main contribution of this study is a non-iterative method for parameter estimation of 2R-1C models appropriate for low-cost and widely used microcontroller-based devices. The proposed method enables reduction of the number of measurement points by 80% compared to the previously proposed non-iterative method while maintaining the same estimation accuracy. More importantly, the proposed method is 30–45 times faster than the state-of-the-art Levenberg-Marquardt iterative estimation method. Such an approach ensures high system portability and autonomy, which is very

important for applications where handheld devices are needed for real-time estimation at the measurement site.

2 Low-complexity methods for parameter estimation of the 2R-1C model

2.1 Non-iterative parameter estimation method

The real and imaginary parts of the complex impedance of the 2R-1C model can be written as

$$R(\omega) = \text{Re}\{\underline{Z}(\omega)\} = K \frac{\omega^2 + zp}{\omega^2 + p^2}, \quad (5)$$

$$X(\omega) = \text{Im}\{\underline{Z}(\omega)\} = K \frac{(p - z)\omega}{\omega^2 + p^2}, \quad (6)$$

where K , z , and p are as follows:

$$K = \frac{R_1 R_2}{R_1 + R_2}, \quad (7)$$

$$z = \frac{1}{R_2 C_2}, \quad (8)$$

$$p = \frac{1}{(R_1 + R_2)C_2}. \quad (9)$$

It is easy to show that the first derivative of $X(\omega)$ is equal to zero for

$$\omega_c = \frac{1}{(R_1 + R_2)C_2}. \quad (10)$$

This frequency is the characteristic angular frequency of the 2R-1C model, which is equal to the reciprocal value of the time constant $\tau = (R_1 + R_2)C_2$. From Eq. (9), we can see that $\omega_c = p$.

The non-iterative parameter estimation (NIPE) method, a non-iterative approach for estimating the parameters of the 2R-1C model (\hat{R}_1 , R_2 , and C_2), was proposed in Simić et al. (2016). In the NIPE method, the estimated value \hat{p} of the characteristic angular frequency is obtained as the frequency where the magnitude of the measured imaginary part of the impedance attains a maximum value. Then parameters $\hat{z}(\omega_i)$ and $\hat{K}(\omega_i)$ are calculated for each measurement angular frequency ω_i as

$$\hat{z}(\omega_i) = \frac{R(\omega_i) \cdot \hat{p} \cdot \omega_i - X(\omega_i) \cdot \omega_i^2}{R(\omega_i) \cdot \omega_i + X(\omega_i) \cdot \hat{p}}, \quad (11)$$

$$\hat{K}(\omega_i) = \frac{R(\omega_i) \cdot \omega_i + X(\omega_i) \cdot \hat{p}}{\omega_i}, \quad (12)$$

where $i = 1, 2, \dots, N$ with N being the total number of data points.

With known \hat{p} , $\hat{K}(\omega_i)$, and $\hat{z}(\omega_i)$, from Eqs. (7)–(9), parameters of the 2R-1C model can be calculated as

$$\hat{R}_1(\omega_i) = \frac{\hat{z}(\omega_i) \cdot \hat{K}(\omega_i)}{\hat{p}}, \quad (13)$$

$$\hat{R}_2(\omega_i) = \frac{\hat{z}(\omega_i) \cdot \hat{K}(\omega_i)}{\hat{z}(\omega_i) - \hat{p}}, \quad (14)$$

$$\hat{C}_2(\omega_i) = \frac{\hat{z}(\omega_i) - \hat{p}}{\hat{z}^2(\omega_i) \cdot \hat{K}(\omega_i)}, \quad (15)$$

for each ω_i ($i = 1, 2, \dots, N$). Finally, the estimated values \hat{R}_1 , \hat{R}_2 , and \hat{C}_2 are obtained as means of $\hat{R}_1(\omega_i)$, $\hat{R}_2(\omega_i)$, and $\hat{C}_2(\omega_i)$ ($i = 1, 2, \dots, N$), respectively.

Compared to the iterative approaches, the advantages of the NIPE method are acceptable estimation accuracy, lower computational complexity, shorter processing time, as well as suitability for portable low-cost microcontroller-based systems and in-situ parameter estimation in real time (Simić et al., 2016). Comprehensive analysis regarding the estimation accuracy and execution time showed that the NIPE method in comparison with the complex nonlinear least squares (CNLS) approach was 20–80 times faster, while still providing an acceptable estimation error that was lower than 1% (Simić et al., 2016). However, in Simić et al. (2016) the estimation accuracy showed a strong dependence on the number of measurement points, with a high number of measurement points required for a satisfactorily accurate estimation of the characteristic frequency.

In the rest of this section we will present the quadratic interpolation non-iterative parameter estimation (QINIPE) method, an approach for reducing the need for a high number of measurement points while keeping the same estimation accuracy without a significant increase in algorithm complexity.

2.2 Quadratic interpolation non-iterative parameter estimation method

The accuracy of characteristic frequency estimation based on finding the maximum magnitude (peak of the curve) of the imaginary part of the impedance can be affected by noise or a limited number of available measurements. In this study, we assume that noise affects both the iterative and non-iterative

methods in the same way and propose a method which will preserve the accuracy of the 2R-1C model parameter estimation with a decreased number of measurements. We leave a detailed analysis of the influence of noise on the 2R-1C model parameter estimation methods and design of appropriate filters for future work.

The influence of uncertainty in the characteristic frequency on the estimated values of the model parameters is very important. It can be observed if instead of the exact value of the characteristic frequency for the given 2R-1C model, the value $\hat{p} = \mu \cdot p$ where μ is a real valued parameter, is used for the estimation of the model parameters. Relative errors for estimated values $\hat{z}(\omega_i)$ and $\hat{K}(\omega_i)$ can be calculated:

$$\begin{aligned} \delta z(\omega_i) &= \frac{\hat{z}(\mu \cdot p, \omega_i) - z}{z} \\ &= \frac{p \cdot \omega_i (1 - \mu) \left(X^2(\omega_i) + R^2(\omega_i) \right)}{\left(\omega_i R(\omega_i) + \mu p X(\omega_i) \right) \left(\omega_i X(\omega_i) - p R(\omega_i) \right)}, \end{aligned} \quad (16)$$

$$\begin{aligned} \delta K(\omega_i) &= \frac{\hat{K}(\mu \cdot p, \omega_i) - K}{K} \\ &= \frac{p \cdot (\mu - 1) \cdot X(\omega_i)}{p \cdot X(\omega_i) + \omega_i \cdot R(\omega_i)}. \end{aligned} \quad (17)$$

Calculations of the relative errors for the estimated values of \hat{R}_1 , \hat{R}_2 , and \hat{C}_2 can be done in a similar way. However, keeping in mind that the estimated values of the model parameters are means of Eqs. (13)–(15), and, therefore, frequency independent, it is more useful to calculate the relative errors as

$$\delta \hat{R}_1 = \frac{\frac{1}{N} \sum_{i=1}^N \hat{R}_1(\omega_i) - R_1}{R_1} = \frac{\hat{R}_1 - R_1}{R_1}, \quad (18)$$

$$\delta \hat{R}_2 = \frac{\frac{1}{N} \sum_{i=1}^N \hat{R}_2(\omega_i) - R_2}{R_2} = \frac{\hat{R}_2 - R_2}{R_2}, \quad (19)$$

$$\delta \hat{C}_2 = \frac{\frac{1}{N} \sum_{i=1}^N \hat{C}_2(\omega_i) - C_2}{C_2} = \frac{\hat{C}_2 - C_2}{C_2}, \quad (20)$$

where R_1 , R_2 , and C_2 are the actual values of the model parameters, while $\hat{R}_1(\omega_i)$, $\hat{R}_2(\omega_i)$, and $\hat{C}_2(\omega_i)$ are defined with Eqs. (13), (14), and (15), respectively.

The number of measurement frequencies N is usually limited by the complexity of the used mea-

surement and data acquisition units, and their capabilities for handling a wide frequency range, small frequency step, and large amount of data. However, in many applications a large number of measurement frequencies are required to allow identification and analysis of the processes involved. Thus, optimization of the number of measurement points is a very important and not easily accomplished task.

In the rest of the study, we use the more convenient f (Hz) instead of ω (rad/s) for specifying the frequency range and characteristic frequency of an impedance. To analyze the influence of the number of measurement points N on characteristic frequency estimation, we consider the frequency range (f_{\min} , f_{\max}). The frequency step is thus

$$\Delta f = \frac{f_{\max} - f_{\min}}{N - 1}. \quad (21)$$

In Fig. 3 the locations of several measurement points on the typical curve $X(f)$ for a 2R-1C model are given. Let the characteristic frequency f_c be located between the two measurement points (f_i , f_{i+1}). The largest possible absolute error in characteristic frequency estimation is $\hat{f}_c - f_c = 0.5\Delta f$.

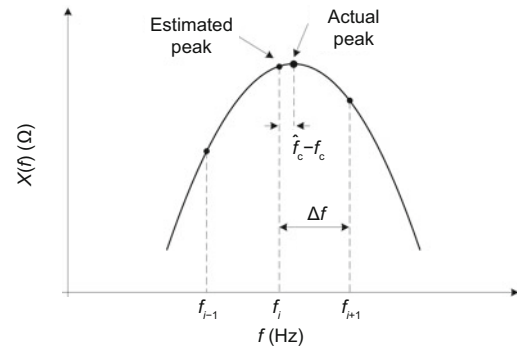


Fig. 3 Error in characteristic frequency estimation due to the limited number of measurement frequencies

Let the maximum acceptable relative error of the characteristic frequency estimation be δf_c . The number of measurement frequencies needed to satisfy this requirement can be calculated from

$$\delta f_c = \frac{\hat{f}_c - f_c}{f_c} = \frac{0.5\Delta f}{f_c} = \frac{f_{\max} - f_{\min}}{2f_c(N - 1)}, \quad (22)$$

as

$$N = 1 + \frac{f_{\max} - f_{\min}}{2 \cdot f_c \cdot \delta f_c}, \quad (23)$$

and the required frequency step is

$$\Delta f = 2 \cdot \delta f_c \cdot f_c. \quad (24)$$

From Eq. (23), we can see that the highest number of measurement frequencies is required if the characteristic frequency is equal to the lower frequency limit, i.e., $f_c = f_{\min}$.

The number of measurement frequencies and frequency step calculated by Eqs. (23) and (24) can be used to ensure that the relative error of the characteristic frequency estimation is smaller than the maximum acceptable value δf_c . However, if $(f_{\min} + h\Delta f) \approx f_c$, where h is an integer, it is possible to obtain an even smaller relative error with fewer measurement frequencies. For example, if the analyzed frequency range is from 10 to 100 kHz, and the characteristic frequency is $f_c=50$ kHz, then $N=10$, corresponding to the frequency step of $\Delta f = 10$ kHz, will cause a smaller error in characteristic frequency estimation than $N = 16$, which corresponds to the frequency step of $\Delta f=6$ kHz. Therefore, it is not easy to predict the optimal value of N that will minimize the estimation error.

A limited number of measurement frequencies leads to a possibility that the measurement point equaling the characteristic frequency is missed in a frequency sweep (Fig. 3). To improve the accuracy of characteristic frequency estimation, we need more accurate estimation of the maximum value of the imaginary part of the impedance. To this end, we propose the QINIPE method which uses a three-point quadratic interpolation around the estimated peak (Fig. 4).

Let

$$X(\omega_{n-1}) = \alpha, \quad (25)$$

$$X(\omega_n) = \beta, \quad (26)$$

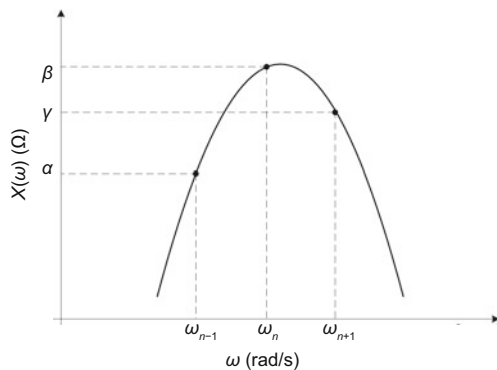


Fig. 4 Values of the imaginary part of impedance around peak β

$$X(\omega_{n+1}) = \gamma. \quad (27)$$

Angular frequency ω_n can be determined from measured data $X(\omega_i)$ ($i = 1, 2, \dots, N$), as the angular frequency at which the absolute value of the imaginary part of impedance has the maximum value. Thus, procedures for finding ω_n involve solving for the maximum value in an array $|X(\omega_i)|$. After ω_n is found, β can be calculated by Eq. (26). Furthermore, neighboring frequencies (ω_{n-1} and ω_{n+1}) can be used to define α and γ , according to Eqs. (25) and (27), respectively.

Solving the set of Eqs. (25)–(27) using a quadratic model for the imaginary part of the impedance

$$a\omega^2 + b\omega + c = X(\omega) \quad (28)$$

gives

$$a = -\frac{(\alpha - \beta)\omega_{n+1} - (\alpha - \gamma)\omega_n + (\beta - \gamma)\omega_{n-1}}{(\omega_{n-1} - \omega_n)(\omega_{n-1} - \omega_{n+1})(\omega_n - \omega_{n+1})}, \quad (29)$$

$$b = -\frac{\alpha(\omega_n^2 - \omega_{n+1}^2) - \beta(\omega_{n-1}^2 - \omega_{n+1}^2)}{(\omega_{n-1} - \omega_n)(\omega_{n-1} - \omega_{n+1})(\omega_n - \omega_{n+1})} - \frac{\gamma(\omega_{n-1}^2 - \omega_n^2)}{(\omega_{n-1} - \omega_n)(\omega_{n-1} - \omega_{n+1})(\omega_n - \omega_{n+1})}, \quad (30)$$

$$c = \frac{(\alpha - \gamma)\omega_{n-1} \cdot \omega_n}{(\omega_{n-1} - \omega_n)(\omega_{n-1} - \omega_{n+1})} - \frac{\alpha \cdot \omega_n - \beta \cdot \omega_{n-1}}{\omega_{n-1} - \omega_n} - \frac{(\beta - \gamma)\omega_{n-1} \cdot \omega_n}{(\omega_{n-1} - \omega_n)(\omega_n - \omega_{n+1})}. \quad (31)$$

The proposed QINIPE method uses the calculated parameters a , b , and c to improve the estimation of the peak of the imaginary part of the impedance, which results in the corrected value of the characteristic angular frequency:

$$\hat{p}_{\text{corr}} = -\frac{b}{2a}. \quad (32)$$

The rest of the QINIPE method is the same as that of the NIPE method, but instead of \hat{p} , the corrected estimate of the characteristic angular frequency \hat{p}_{corr} is used in Eqs. (11)–(15) for estimation of the 2R-1C model parameters.

The innovative aspect of this work is that we suggest an improvement of the previously reported method for parameter estimation of the 2R-1C model, making it more suitable for low-cost embedded hardware. The benefits of such a realization are

higher accuracy and lower complexity with a very short processing time, which makes it interesting for portable and low-cost diagnostic devices.

3 Experimental results and discussion

As a part of the validation process of the non-iterative methods described in Section 2, we first analyze the accuracy of the parameter estimation of 2R-1C models with numerically calculated (simulated) impedance data. After that, we compare the microcontroller-based implementations of the QINIFE and NIPE methods. Finally, the proposed QINIFE method is compared to the CNLS method on the real impedance data.

3.1 Simulation

3.1.1 Data generation

To analyze the influence of the uncertainty in characteristic frequency estimation and the number of measurement points on model parameter estimation, the reference values chosen for simulation are $R_1 = 1 \text{ k}\Omega$, $R_2 = 470 \text{ }\Omega$, and $C_2 = 4.7 \text{ nF}$. These values are chosen because of the availability of components for hardware-based experiments. The characteristic angular frequency of the analyzed 2R-1C model calculated using Eq. (10) for the given reference values is $\omega_c = 144\,738.750 \text{ rad/s}$, while the corresponding characteristic frequency is $f_c = 23\,035.887 \text{ Hz}$. The complex impedance data are calculated using Eq. (1) in the frequency range from 5 to 100 kHz, which is common for low-cost and widely used microcontroller-based impedance meters (Seoane et al., 2008). Additionally, for more quantitative characterization of the non-iterative methods, we use a simulated impedance of the 2R-1C models with reference values estimated from six common electrical bioimpedance (EBI) measurements: total body composition (TBC), respiration rate (RR), trunk-trunk (TT), leg-leg (LL), lung composition (LC), and arm-arm (AA) (Pena, 2009; Ferreira et al., 2010).

3.1.2 Influence of uncertainty in characteristic frequency on the estimated values of model parameters

Instead of the actual values for the characteristic frequency, we used values of $\mu \in \{\pm 0.01, \pm 0.02, \pm 0.05, \pm 0.1\}$. Thus, we introduced

relative errors, δf_c (%), in characteristic frequency estimations of $\pm 1\%$, $\pm 2\%$, $\pm 5\%$, and $\pm 10\%$, respectively. Additionally, we wanted to analyze if the sign of the relative error in characteristic frequency estimation influences the estimated values of the model parameters. The numbers of measurement frequencies (10, 100, and 1000) were chosen arbitrarily to cover the analyzed frequency range. The estimated values of the model parameters using the NIPE method are presented in Table 1.

Table 1 Relative errors for estimated values of model parameters for different δf_c and N

N	δf_c (%)	δR_1 (%)	δR_2 (%)	δC_2 (%)
10	10	-4.338	-6.853	-4.130
100	10	-4.475	-6.202	-4.253
1000	10	-4.488	-6.141	-4.265
10	5	-2.272	-3.486	-2.151
100	5	-2.344	-3.134	-2.217
1000	5	-2.351	-3.101	-2.223
10	2	-0.936	-1.409	-0.881
100	2	-0.965	-1.262	-0.910
1000	2	-0.968	-1.248	-0.913
10	1	-0.473	-0.707	-0.445
100	1	-0.487	-0.632	-0.459
1000	1	-0.489	-0.625	-0.460
10	-1	0.482	0.712	0.452
100	-1	0.498	0.635	0.467
1000	-1	0.499	0.627	0.468
10	-2	0.974	1.429	0.913
100	-2	1.005	1.272	0.942
1000	-2	1.008	1.258	0.945
10	-5	2.512	3.612	2.342
100	-5	2.591	3.199	2.418
1000	-5	2.598	3.161	2.425
10	-10	5.303	7.359	4.898
100	-10	5.469	6.462	5.060
1000	-10	5.485	6.379	5.075

As can be seen from Table 1, the relative errors in estimation of parameters were within $[-1\%, +1\%]$ if δf_c was $\pm 1\%$. Moreover, if $\mu < 0$ the relative errors were positive; otherwise, they were negative. The number of measurement frequencies did not make a significant difference in the estimated values of the model parameters. Therefore, it is important only for the estimation of the characteristic frequency. Relative errors in the estimation of values of the model parameters up to 1% are usually acceptable in many practical cases, and we will

consider that case in the remainder of the study. Thus, our target is the estimation of the characteristic frequency with relative errors less than 1%.

3.1.3 Influence of the number of measurement points on characteristic frequency estimation

If the analyzed frequency range is from 5 to 100 kHz and required $\delta f_c = 0.01$ (1% error), the highest number of measurement points is required if $f_c=5$ kHz. According to Eq. (23) the required number of measurement points is $N = 951$ (frequency step of 100 Hz). Using the NIPE method the estimated value of the characteristic frequency of the analyzed 2R-1C model was $\hat{f}_c = 23.000$ kHz. Thus, the characteristic frequency was estimated with a relative error of -0.156% . The estimated value of the characteristic frequency was used for parameter estimation of the analyzed 2R-1C model. As expected, the values of model parameters $\hat{R}_1 = 1000.770 \Omega$, $\hat{R}_2 = 470.459 \Omega$, and $\hat{C}_2 = 4.703$ nF were estimated with very small relative errors, that is, $\delta R_1 = 0.077\%$, $\delta R_2 = 0.098\%$, and $\delta C_2 = 0.072\%$.

However, the relatively high number of measurement points required for the frequency step of 100 Hz is not suitable for low-cost impedance meters because an advanced data acquisition unit and high processing time are required. Moreover, in many practical applications (Blad, 1996), characteristic frequency is usually a few tens of kHz, which can significantly reduce the required number of measurement frequencies. For example, studies of bioimpedance have shown that the mean values of characteristic frequencies are 80.1 and 57 kHz for women and men, respectively (de Lorenzo et al., 1997; Ward et al., 2000; Kyle et al., 2001; Schulz et al., 2006). The median values of characteristic frequencies are 32 kHz for men and 35 kHz for women (Ward and Heitmann, 1998). Thus, apriori knowledge about the analyzed system is very useful in reducing the required number of measurement points. Moreover, the approximate location of the characteristic frequency can be found by means of an initial impedance measurement (screening) with just a few measurement points. For example, if the minimum possible f_c is 20 kHz, then according to Eq. (23), $N = 238$ should ensure a less than 1% error in characteristic frequency estimation.

Using the NIPE method, the estimated value of the characteristic frequency of the analyzed 2R-1C model when $N = 238$ is $\hat{f}_c = 23\,037.975$ Hz. Thus,

the characteristic frequency was estimated with an error of 0.009%. This estimated value was used for parameter estimation of the analyzed 2R-1C model. As expected, the values of the model parameters $\hat{R}_1 = 999.955 \Omega$, $\hat{R}_2 = 469.973 \Omega$, and $\hat{C}_2 = 4.700$ nF were estimated with very small relative errors, i.e., $\delta R_1 = -0.004\%$, $\delta R_2 = 0.040\%$, and $\delta C_2 = 0.004\%$.

3.1.4 Characteristic frequency estimation of the 2R-1C model using the QINIPE method

As mentioned before, our approach described in Section 2.2 aims to reduce the number of measurement points while keeping a high accuracy in the estimation of the model parameters. To this end, we used quadratic interpolation of the measurement values around the peak of the imaginary part of the measured impedance. We started with $N = 238$, and then N was decreased to 3, as the minimum number of measurement points needed to implement quadratic interpolation. For each tested number of measurements, the value of parameter p was estimated using Eqs. (29)–(32) while δf_c was monitored. As can be seen in Fig. 5, using the QINIPE method it is possible to reduce N to 29 while keeping the relative error in the characteristic frequency estimation lower than 1%. In contrast, a much higher number of measurement frequencies ($N = 173$) was required for the NIPE method. Additionally, for $N = 29$ the relative error in characteristic frequency estimation using the NIPE method was 4.652%, much higher than 0.683% obtained using the QINIPE method.

The NIPE and QINIPE methods were also compared regarding relative errors in the estimated values of model parameters. The relative errors in

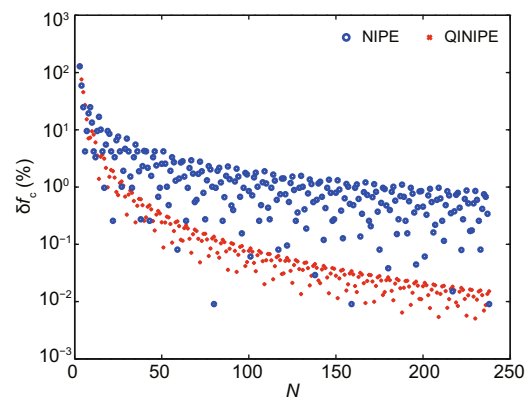


Fig. 5 Comparison of relative errors in characteristic frequency estimation

parameter estimation for different numbers of measurement frequencies are shown in Figs. 6–8. From Figs. 6–8, we can see that, using the QINIFE method it is possible to have a 1% relative error in parameter estimation with 80% fewer measurement points ($N = 23$) compared to the NIPE method ($N = 115$).

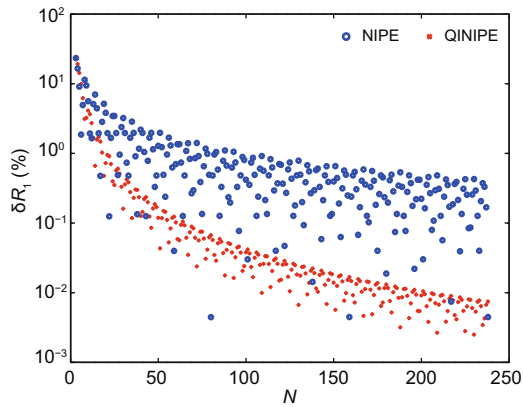


Fig. 6 Comparison of relative errors in estimation of R_1

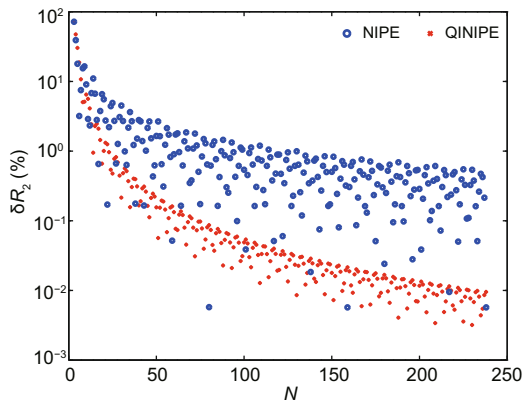


Fig. 7 Comparison of relative errors in estimation of R_2

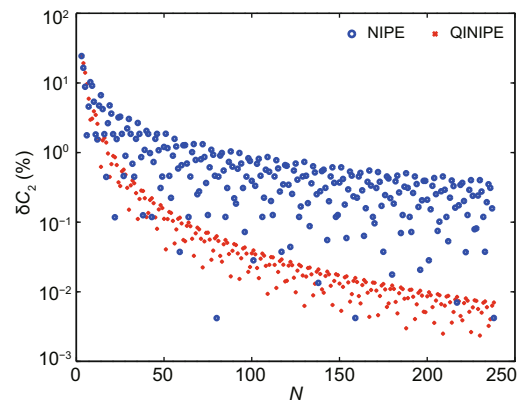


Fig. 8 Comparison of relative errors in estimation of C_2

3.1.5 Parameter estimation of the 2R-1C model from simulated bioimpedance

To obtain more quantitative characterization of the proposed method, we performed parameter estimation using simulated impedances of 2R-1C models whose reference values were estimated from six common EBI measurements: TBC, RR, TT, LL, LC, and AA. The reference values for the model parameters as well as the characteristic frequencies are shown in Table 2.

The values from Table 2 were used to calculate the reference impedance data in the frequency range from 5 to 100 kHz. The experiment started with $N = 951$ and then the number of measurement frequencies was decreased with the aim of comparing the required numbers of measurements needed to have the relative estimation errors of all three model parameters lower than 1%. The NIPE and QINIFE methods were used on the same dataset and the results obtained are presented in Fig. 9.

As can be seen from Fig. 9, the QINIFE method enabled a reduction of the number of measurement points of more than 80% in comparison to the NIPE

Table 2 Reference values for model parameters (Pena, 2009; Ferreira et al., 2010)

EBI	R_1 (Ω)	R_2 (Ω)	C_2 (nF)	f_c (Hz)
TBC	917.50	629.00	3.42	30 091.52
RR	58.50	23.90	75.70	25 515.09
TT	99.00	42.30	44.00	25 599.14
LL	510.00	450.00	6.55	25 310.90
LC	81.46	19.64	47.70	33 002.79
AA	364.60	379.00	6.20	34 521.45

EBI: electrical bioimpedance; TBC: total body composition; RR: respiration rate; TT: trunk-trunk; LL: leg-leg; LC: lung composition; AA: arm-arm

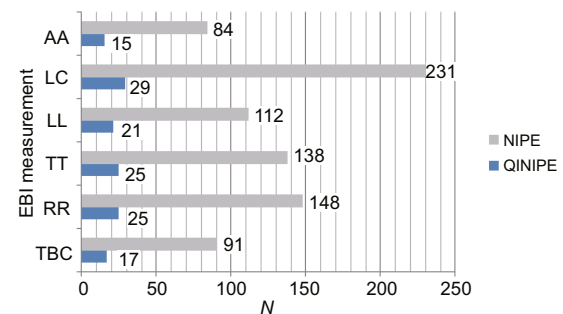


Fig. 9 Comparison of the minimum number of measurement points required for relative errors lower than 1%

TBC: total body composition; RR: respiration rate; TT: trunk-trunk; LL: leg-leg; LC: lung composition; AA: arm-arm

method, while achieving an estimation error for all three model parameters lower than 1%.

Furthermore, we compared the execution time of the described non-iterative methods as well as the CNLS. Our test platform was MATLAB R2013b installed on a Lenovo notebook with an i5-4300M CPU at 2.60 GHz and a 64-bit Windows 7 operating system. For CNLS estimation, the Levenberg-Marquardt algorithm was used as implemented in the MATLAB function `lsqcurvefit`. The maximum numbers of function evaluations and iterations were set to 10^3 , while the termination tolerance on the function value and that on the estimated vector were set to 10^{-4} . To increase the speed of estimation, analytical expressions for the Jacobian matrix were supplied to the solver. By measuring the performances using a stopwatch timer (MATLAB commands `tic` and `toc`), we determined that the QINIFE method requires a slightly higher processing time than NIPE (Table 3). However, it required a significantly lower number of measurement points for 1% error, which can be a huge advantage if low-cost microcontroller-based devices are used. In addition, when compared to CNLS, the relative estimation errors of both QINIFE and NIPE were higher, but the QINIFE was 30–45 times faster.

Table 3 Comparison of execution time

EBI	N			t (ms)		
	NIPE	QINIFE	CNLS	NIPE	QINIFE	CNLS
TBC	91	17	17	4.561	5.060	180.621
RR	148	25	25	5.067	5.949	190.501
TT	138	25	25	5.865	7.037	190.925
LL	112	21	21	3.386	4.480	193.935
LC	231	29	29	3.298	4.085	179.834
AA	84	15	15	3.871	3.895	186.247

EBI: electrical bioimpedance; TBC: total body composition; RR: respiration rate; TT: trunk-trunk; LL: leg-leg; LC: lung composition; AA: arm-arm

3.2 Microcontroller-based experiment

The AD5933-based impedance measurement system (Fig. 10) reported in Simić et al. (2017b) was used for impedance measurement of the analyzed 2R-1C model. The device is based on an 8-bit ATmega128 microcontroller and integrated circuit AD5933. Communication between the microcontroller and AD5933 (device initialization, definition of measurement details, and collection of measurement data) is via the inter-integrated circuit (I2C)

protocol. Using this device it is possible to perform frequency sweep impedance measurement in the frequency range from 5 to 100 kHz with a maximum of 511 points and a frequency step as low as 0.1 Hz.

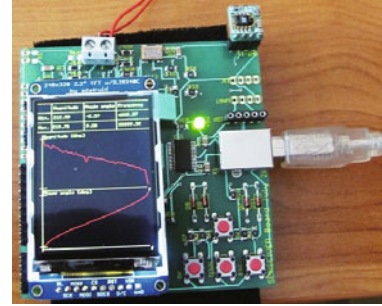


Fig. 10 AD5933-based impedance measurement device

Tests of accuracy of the developed impedance measurement device were performed using series and parallel R-C networks, with values for R and C chosen in such a way to ensure a wide range of impedance magnitudes and phase angle changes. The results obtained were compared to the reference measurement results obtained using an Agilent 4263B LCR meter and Hewlett Packard 4194A Impedance/Gain-Phase Analyzer. For impedance magnitude in the range from 100 Ω to 100 k Ω , the maximum system errors for magnitude and phase angle measurements in the complete frequency range were less than 3% and 2.5°, respectively (Simić, 2014; Simić and Stojanović, 2017).

To apply the developed device in real-time impedance measurement, it is necessary to investigate how long it takes to collect impedance data for one measurement point. The theoretical sample time for a single measurement using AD5933 is the sum of the following three parts (Ferreira et al., 2013):

1. The time required for the AD5933 to estimate the impedance values, which is approximately 1 ms for a commonly used system clock of 16 MHz.
2. The total time to perform all the I2C protocol instructions.
3. The settling cycle time (the total number of settling cycles multiplied by the period of the excitation signal).

For the I2C frequency at 400 kHz, one settling cycle, and excitation frequency of 50 kHz, the theoretical impedance sampling time is 1.895 ms, while the experimentally obtained time needed to

perform all the operations required for one measurement at 50 kHz is around 1.7910 ms (Ferreira et al., 2013), and for the excitation frequency at 100 kHz it is around 1.7911 ms (Ferreira et al., 2013). The experimentally obtained values are means calculated for 100 repeated measurements.

The 2R-1C model was implemented with real components using the same nominal values as used in the simulation part, namely, $R_1 = 1000 \Omega (\pm 5\%)$, $R_2 = 470 \Omega (\pm 5\%)$, and $C_2 = 4.7 \text{ nF} (\pm 5\%)$. With these values, the nominal characteristic frequency calculated using Eq. (10) is 23 035.887 Hz. Using the AD5933-based measurement device, the impedances of the used components in the frequency range from 5 to 100 kHz were measured. The results obtained (mean values \pm standard deviation) were $R_1 = 983.37 \pm 0.67 \Omega$, $R_2 = 463.49 \pm 1.22 \Omega$, and $C_2 = 4.55 \pm 0.06 \text{ nF}$. Using the mean values the calculated characteristic frequency is 24 175.876 Hz. It can be seen that there is a slight difference in comparison with the nominal values of the model parameters and characteristic frequency.

The impedance measurement of the 2R-1C model was performed in the frequency range from 5 to 100 kHz at 29 frequency points, because in the simulation $N = 29$ was shown to be the required number of measurements needed to achieve a 1% relative error in characteristic frequency estimation using quadratic interpolation.

We also compared the microcontroller-based implementations (https://github.com/simicm1987/2R1C_estimation) of the NIPE and QINIPE methods. Our test platform was Arduino Uno board based on the ATmega328P microcontroller with 2 KB SRAM, 16 MHz clock speed, and 32 KB flash memory in total. The estimated values of the characteristic frequency, the mean values of the model parameters \hat{R}_1 , \hat{R}_2 , and \hat{C}_2 , and the standard deviations σR_1 , σR_2 , and σC_2 obtained using the NIPE and QINIPE methods are shown in Table 4.

As shown in Table 4, the standard deviations of

the mean values \hat{R}_1 , \hat{R}_2 , and \hat{C}_2 , estimated using the NIPE method, were 1.419%, 2.337%, and 0.406%, respectively. Using the QINIPE method these values were 0.852%, 1.167%, and 0.913%, respectively. The estimated values of $\hat{R}_1(f)$, $\hat{R}_2(f)$, and $\hat{C}_2(f)$ at different frequencies normalized to the estimated mean values (\hat{R}_1 , \hat{R}_2 , and \hat{C}_2) are shown in Figs. 11–13.

The values estimated using the NIPE and QINIPE methods were then used to calculate the impedances of the 2R-1C model (Eq. (4)) at 29 points in the frequency range from 5 to 100 kHz. Because of the tolerances of the nominal values, the frequency-dependent characteristics of the deployed components, the measurement noise, and the actual reference values for the model parameters were not known. Therefore, we chose to compare the measured impedance and the impedance calculated using the estimated values of the model parameters (Fig. 14).

The relative errors $\delta R(\omega)$ (%) and $\delta X(\omega)$ (%) for the real and imaginary parts of the estimated impedances are shown in Figs. 15 and 16, respectively.

As can be seen from Figs. 15 and 16, the maximum differences between the measured and impedance calculated using the parameters estimated by means of the QINIPE method were smaller

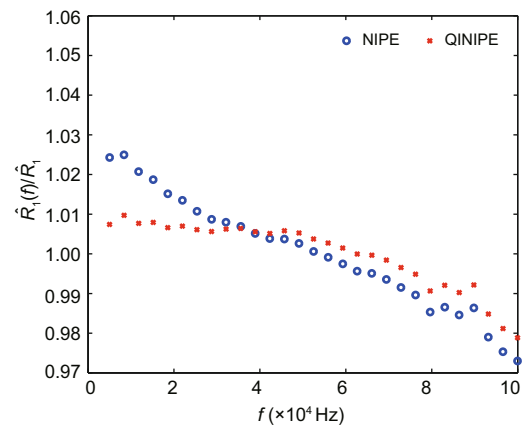


Fig. 11 Normalized $\hat{R}_1(f)$ values

Table 4 Estimated values for the characteristic frequency and model parameters for $N = 29$

Data source	\hat{f}_c (Hz)	$\hat{R}_1 \pm \sigma R_1$ (Ω)	$\hat{R}_2 \pm \sigma R_2$ (Ω)	$\hat{C}_2 \pm \sigma C_2$ (nF)
Nominal values	23 035.887	1000 \pm 0.05	470 \pm 0.05	4.7 \pm 0.05
Measured	24 175.876	983.37 \pm 0.67	463.49 \pm 1.22	4.550 \pm 0.06
NIPE	23 352.000	955.653 \pm 13.563	467.185 \pm 10.916	4.412 \pm 0.018
QINIPE	24 409.671	972.629 \pm 8.290	479.621 \pm 5.647	4.490 \pm 0.04

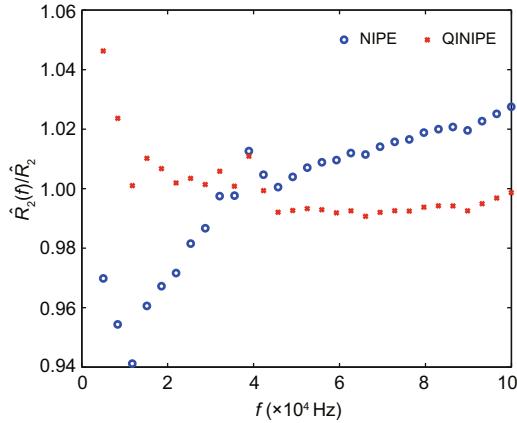


Fig. 12 Normalized $\hat{R}_2(f)$ values

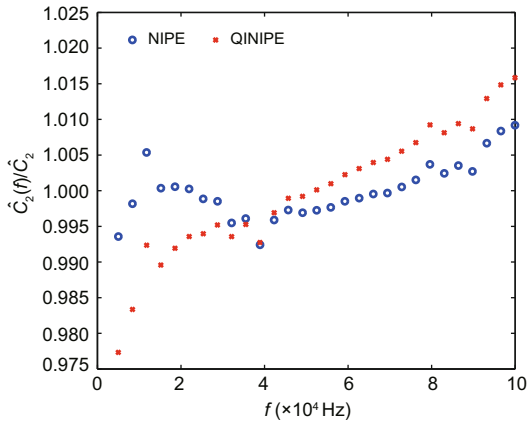


Fig. 13 Normalized $\hat{C}_2(f)$ values

for both the real part ($1.197\% < 2.328\%$) and imaginary part ($2.722\% < 4.667\%$) of the impedance.

Additionally, we compared the root mean square errors (RMSEs) between the measured impedance (R_{meas} and X_{meas}) and impedance calculated (R_{calc} and X_{calc}) using the values of the model parameters obtained using the NIPE and QINIFE methods. The RMSEs for the real and imaginary parts of the impedance were calculated as follows:

$$RMSE_R = \sqrt{\frac{\sum_{i=1}^N (R_{calc}(\omega_i) - R_{meas}(\omega_i))^2}{N}}, \quad (33)$$

$$RMSE_X = \sqrt{\frac{\sum_{i=1}^N (X_{calc}(\omega_i) - X_{meas}(\omega_i))^2}{N}}. \quad (34)$$

The RMSE values obtained are shown in Fig. 17. We can see that the RMSEs for impedance estimated using QINIFE were smaller for 42.8% (real part) and 64.5% (imaginary part) in comparison to the values estimated using NIPE.

Using the Arduino stopwatch timer (function micros) we determined that the NIPE method can

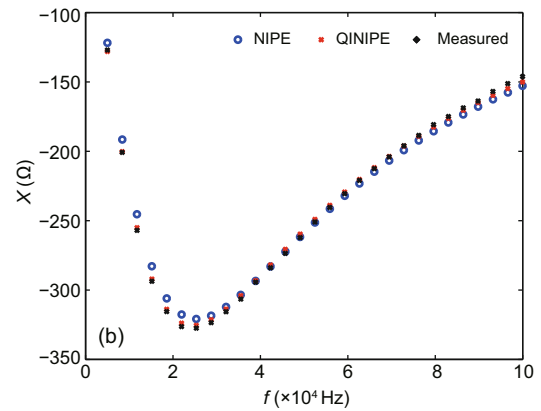
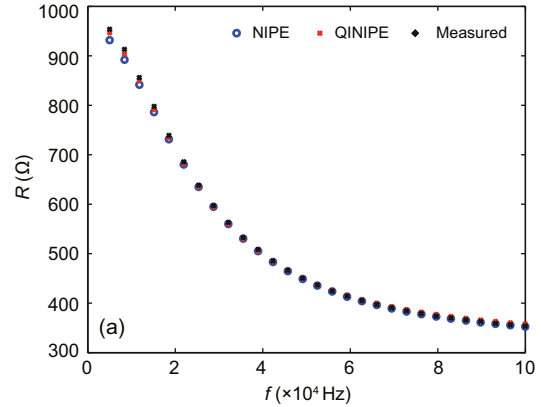


Fig. 14 Comparison of measured impedance and impedance calculated with estimated values of model parameters: (a) real part; (b) imaginary part

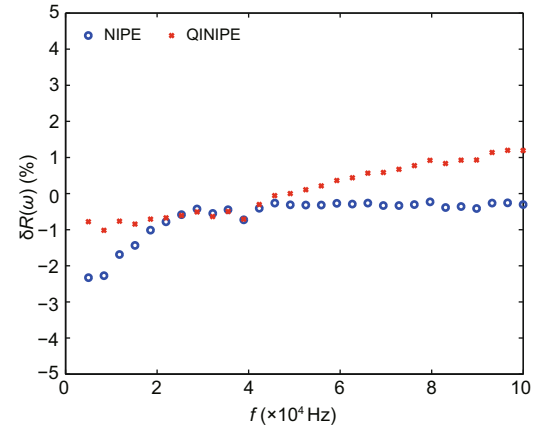


Fig. 15 Comparison of relative errors for the real part of impedance

estimate the parameter values in 8.592 ms, while the QINIFE method required 9.168 ms. The QINIFE method required 6306 bytes of flash memory and 1396 bytes of RAM, while the NIPE method required 5060 bytes of flash memory and 1364 bytes of RAM (Fig. 18).

Although the QINIFE method required 6.7% higher execution time, 24% more flash memory, and

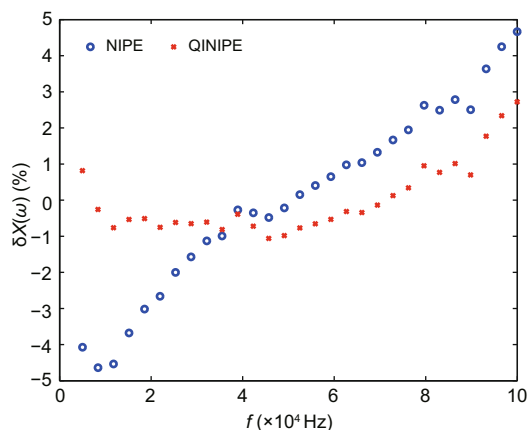


Fig. 16 Comparison of relative errors for the imaginary part of impedance

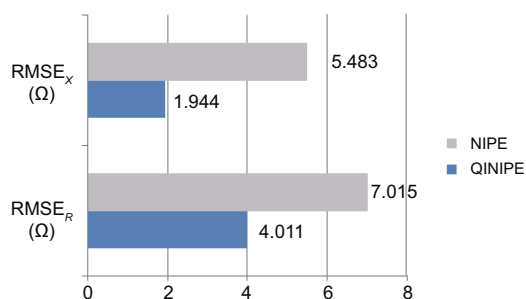


Fig. 17 Comparison of RMSEs for the real and imaginary parts of impedance

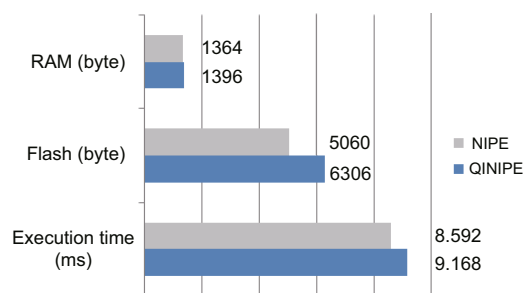


Fig. 18 Performance comparison of the microcontroller implementation of NIPE and QINIPE

2.4% more RAM compared to the NIPE method, it is still acceptable for practical implementations and applications with low-cost microcontroller-based devices.

4 Conclusions

In this study the QINIPE method, suitable for low-cost embedded hardware, has been proposed for estimation of 2R-1C model parameters. The QINIPE model used quadratic interpolation of the

imaginary part of the measured impedance around the initially estimated characteristic frequency to increase the accuracy of characteristic frequency estimation. As a result, the accuracy of estimation of all parameters of the 2R-1C model has been improved. With the known characteristic frequency the 2R-1C model parameters were calculated from the measured real and imaginary parts of an impedance using closed-form expressions.

The performed comparative analysis showed that the proposed QINIPE method reduced the required number of measurement points by 80% in comparison with our previously reported NIPE method without quadratic interpolation, while keeping the estimation errors for all parameters less than 1%. The NIPE and QINIPE methods were implemented on the Arduino Uno board. In comparison to the NIPE method, the execution time of the QINIPE method was slightly increased by 0.576 ms (about 6.7%), and it required 24% (1.2 KB) more flash memory and just 2.4% (32 bytes) more RAM. Microcontroller-based experiments demonstrated the suitability of the proposed method for implementation on low-cost microcontroller-based devices with limited resources for power consumption, computational complexity, and RAM usage, as well as for applications where portable operation is needed.

The proposed algorithm is a step towards the integration of low-cost AD5933-based impedance measurement system with non-iterative approaches in a compact unit for bioimpedance analysis and in-situ sensor parameter estimation in general. Low-complexity algorithms and real-time execution with satisfactory accuracy are the main requirements for such a device. To further improve the performance of this system, we plan to focus on preprocessing of the measured impedance data in future work.

Compliance with ethics guidelines

Mitar SIMIĆ, Zdenka BABIĆ, Vladimir RISOJEVIĆ, and Goran M. STOJANOVIĆ declare that they have no conflict of interest.

References

- Abbasbandy S, 2005. Extended Newton's method for a system of nonlinear equations by modified Adomian decomposition method. *Appl Math Comput*, 170(1):648-656. <https://doi.org/10.1016/j.amc.2004.12.048>
- Al-Ali AA, Elwakil AS, Maundy BJ, et al., 2018. Extraction of phase information from magnitude-only

- bio-impedance measurements using a modified Kramers-Kronig transform. *Circ Syst Signal Process*, 37(8):3635-3650.
<https://doi.org/10.1007/s00034-017-0727-y>
- Babolian E, Biazar J, Vahidi AR, 2004. Solution of a system of nonlinear equations by Adomian decomposition method. *Appl Math Comput*, 150(3):847-854.
[https://doi.org/10.1016/S0096-3003\(03\)00313-8](https://doi.org/10.1016/S0096-3003(03)00313-8)
- Barsoukov E, Macdonald JR, 2005. Impedance Spectroscopy: Theory, Experiment, and Applications. John Wiley & Sons, Inc., USA.
- Bertrand CA, Hopfer U, 2002. Measurement of membrane capacitance in epithelial monolayers. In: Wise C (Ed.), *Epithelial Cell Culture Protocols*. Humana Press, p.315-327. <https://doi.org/10.1385/1-59259-185-X:315>
- Blad B, 1996. Clinical applications of characteristic frequency measurements: preliminary *in vivo* study. *Med Biol Eng Comput*, 34(5):362-365.
<https://doi.org/10.1007/BF02520006>
- Boinet M, Condolf C, Goulet R, et al., 2016. Parameter identification in electrochemical impedance spectroscopy applications: analysis of sensitivity. *Meet Abstr*, MA2016-02:1707.
- Bondarenko AS, 2012. Analysis of large experimental datasets in electrochemical impedance spectroscopy. *Anal Chim Acta*, 743:41-50.
<https://doi.org/10.1016/j.aca.2012.06.055>
- Boukamp BA, Rolle A, 2018. Use of a distribution function of relaxation times (DFRT) in impedance analysis of SOFC electrodes. *Sol State Ion*, 314:103-111.
<https://doi.org/10.1016/j.ssi.2017.11.021>
- Cordero A, Torregrosa JR, 2007. Variants of Newton's method using fifth-order quadrature formulas. *Appl Math Comput*, 190(1):686-698.
<https://doi.org/10.1016/j.amc.2007.01.062>
- Darvishi MT, Barati A, 2007. A third-order Newton-type method to solve systems of nonlinear equations. *Appl Math Comput*, 187(2):630-635.
<https://doi.org/10.1016/j.amc.2006.08.080>
- de Lorenzo A, Andreoli A, Matthie J, et al., 1997. Predicting body cell mass with bioimpedance by using theoretical methods: a technological review. *J Appl Physiol*, 82(5):1542-1558.
<https://doi.org/10.1152/jappl.1997.82.5.1542>
- Dong TK, Kirchev A, Mattera F, et al., 2011. Dynamic modeling of Li-ion batteries using an equivalent electrical circuit. *J Electrochem Soc*, 158(3):A326-A336.
- Ferreira J, Seoane F, Ansele A, et al., 2010. AD5933-based spectrometer for electrical bioimpedance applications. *J Phys*, 224(1):012011.
<https://doi.org/10.1088/1742-6596/224/1/012011>
- Ferreira J, Seoane F, Lindercrantz K, 2013. Portable bioimpedance monitor evaluation for continuous impedance measurements. Towards wearable plethysmography applications. Proc 35th Annual Int Conf of the IEEE Engineering in Medicine and Biology Society, p.559-562.
<https://doi.org/10.1109/EMBC.2013.6609561>
- Freeborn TJ, Elwakil AS, Maundy B, 2017. Variability of cole-model bioimpedance parameters using magnitude-only measurements of apples from a two-electrode configuration. *Int J Food Prop*, 20(S1):S507-S519.
<https://doi.org/10.1080/10942912.2017.1300810>
- Gheorghe AG, Marin CV, Constantinescu F, et al., 2012. Parameter identification for a new circuit model aimed to predict body water volume. *Adv Electr Comput Eng*, 12(4):83-86.
<https://doi.org/10.4316/AECE.2012.04013>
- Golbabai A, Javidi M, 2007. A new family of iterative methods for solving system of nonlinear algebraic equations. *Appl Math Comput*, 190(2):1717-1722.
<https://doi.org/10.1016/j.amc.2007.02.055>
- Holevinsky KO, Nelson DJ, 1998. Membrane capacitance changes associated with particle uptake during phagocytosis in macrophages. *Biophys J*, 75(5):2577-2586.
[https://doi.org/10.1016/S0006-3495\(98\)77703-3](https://doi.org/10.1016/S0006-3495(98)77703-3)
- Hotka M, Zahradnik I, 2014. Membrane capacitance changes due to temperature increase in rat cardiac myocytes. *Biophys J*, 106(2 Suppl 1):121A-122A.
<https://doi.org/10.1016/j.bpj.2013.11.726>
- Kern R, Sastrawan R, Ferber J, et al., 2002. Modeling and interpretation of electrical impedance spectra of dye solar cells operated under open-circuit conditions. *Electrochim Acta*, 47(26):4213-4225.
[https://doi.org/10.1016/S0013-4686\(02\)00444-9](https://doi.org/10.1016/S0013-4686(02)00444-9)
- Kyle UG, Genton L, Slosman DO, et al., 2001. Fat-free and fat mass percentiles in 5225 healthy subjects aged 15 to 98 years. *Nutrition*, 17(7-8):534-541.
[https://doi.org/10.1016/S0899-9007\(01\)00555-X](https://doi.org/10.1016/S0899-9007(01)00555-X)
- Lazović G, Vosika Z, Lazarević M, et al., 2014. Modeling of bioimpedance for human skin based on fractional distributed-order modified cole model. *FME Trans*, 42(1):74-81. <https://doi.org/10.5937/fmet1401075L>
- Manjakkal L, Cvejic K, Kulawik J, et al., 2014. Fabrication of thick film sensitive RuO₂-TiO₂ and Ag/AgCl/KCl reference electrodes and their application for pH measurements. *Sens Actuat B*, 204:57-67.
<https://doi.org/10.1016/j.snb.2014.07.067>
- Manjakkal L, Djurdjic E, Cvejic K, et al., 2015a. Electrochemical impedance spectroscopic analysis of RuO₂ based thick film pH sensors. *Electrochim Acta*, 168:246-255. <https://doi.org/10.1016/j.electacta.2015.04.048>
- Manjakkal L, Cvejic K, Bajac B, et al., 2015b. Microstructural, impedance spectroscopic and potentiometric analysis of Ta₂O₅ electrochemical thick film pH sensors. *Electroanalysis*, 27(3):770-781.
<https://doi.org/10.1002/elan.201400571>
- Maundy BJ, Elwakil AS, Allagui A, 2015. Extracting the parameters of the single-dispersion cole bioimpedance model using a magnitude-only method. *Comput Electr Agric*, 119:153-157.
<https://doi.org/10.1016/j.compag.2015.10.014>
- Moss P, Au G, Plichta EJ, et al., 2008. An electrical circuit for modeling the dynamic response of Li-ion polymer batteries. *J Electrochem Soc*, 155(12):A986-A994.
<https://doi.org/10.1149/1.2999375>
- Noor MA, 2007. Fifth-order convergent iterative method for solving nonlinear equations using quadrature formula. *J Math Contr Sci Appl*, 1:241-249.
- Ortega JM, Rheinboldt WC, 1970. Iterative Solution of Nonlinear Equations in Several Variables. Academic Press, New York, USA.
- Pena AA, 2009. A feasibility study of the suitability of an AD5933-based spectrometer for EBI applications. University of Boras, Boras, p.2009-2010.

- Qiao GF, Wang W, Duan W, et al., 2012. Bioimpedance analysis for the characterization of breast cancer cells in suspension. *IEEE Trans Biomed Eng*, 59(8):2321-2329. <https://doi.org/10.1109/TBME.2012.2202904>
- Ramírez-Chavarría RG, Quintana-Carapia G, Müller MI, et al., 2018. Bioimpedance parameter estimation using fast spectral measurements and regularization. *IFAC-PapersOnLine*, 51(15):521-526. <https://doi.org/10.1016/j.ifacol.2018.09.198>
- Sanchez B, Schoukens J, Bragos R, et al., 2011. Novel estimation of the electrical bioimpedance using the local polynomial method. Application to in vivo real-time myocardium tissue impedance characterization during the cardiac cycle. *IEEE Trans Biomed Eng*, 58(12):3376-3385. <https://doi.org/10.1109/TBME.2011.2166116>
- Sanchez B, Rojas CR, Vandersteen G, et al., 2012. On the calculation of the D -optimal multisine excitation power spectrum for broadband impedance spectroscopy measurements. *Meas Sci Technol*, 23(8):085702. <https://doi.org/10.1088/0957-0233/23/8/085702>
- Sanchez B, Bandarenka AS, Vandersteen G, et al., 2013. Novel approach of processing electrical bioimpedance data using differential impedance analysis. *Med Eng Phys*, 35(9):1349-1357.
- Sánchez Terrones B, Louarroudi E, Pintelon R, et al., 2013. Modeling the non-stationary behaviour of time-varying electrical bioimpedance. Proc 19th IMEKO Symp Measurements of Electrical Quantities, p.378-384.
- Santos-Sacchi J, 2004. Determination of cell capacitance using the exact empirical solution of $\delta Y/\delta C_m$ and its phase angle. *Biophys J*, 87(1):714-727. <https://doi.org/10.1529/biophysj.103.033993>
- Schulz H, Teske D, Penven D, et al., 2006. Fat-free mass from two prediction equations for bioelectrical impedance analysis in a large German population compared with values in Swiss and American adults: reasons for a bi-adata project. *Nutrition*, 22(9):973-975. <https://doi.org/10.1016/j.nut.2006.04.007>
- Seoane F, Ferreira J, Sánchez JJ, et al., 2008. An analog front-end enables electrical impedance spectroscopy system on-chip for biomedical applications. *Physiol Meas*, 29(6):S267-S278. <https://doi.org/10.1088/0967-3334/29/6/S23>
- Simić M, 2014. Complex impedance measurement system for environmental sensors characterization. Proc 22nd Telecommunications Forum Telfor, p.660-663. <https://doi.org/10.1109/TELFOR.2014.7034495>
- Simić M, Stojanović GM, 2017. Compact electronic system for complex impedance measurement and its experimental verification. Proc European Conf on Circuit Theory and Design, p.1-4. <https://doi.org/10.1109/ECCTD.2017.8093360>
- Simić M, Babić Z, Risojević V, et al., 2016. A novel non-iterative method for real-time parameter estimation of the Fricke-Morse model. *Adv Electr Comput Eng*, 16(4):57-62. <https://doi.org/10.4316/AECE.2016.04009>
- Simić M, Babić Z, Risojević V, et al., 2017a. A novel approach for parameter estimation of Fricke-Morse model using differential impedance analysis. Proc Int Conf on Medical and Biological Engineering, p.487-494. https://doi.org/10.1007/978-981-10-4166-2_75
- Simić M, Manjakkal L, Zaraska K, et al., 2017b. TiO₂-based thick film pH sensor. *IEEE Sens J*, 17(2):248-255. <https://doi.org/10.1109/JSEN.2016.2628765>
- Vargas-Bernal R, de la Cruz Blas CA, Gómez-Polo C, 2018. Electrical circuit modeling of sensor magneto-impedances with a square-root frequency dependence. *IEEE Sens J*, 18(2):623-628. <https://doi.org/10.1109/JSEN.2017.2776525>
- Wang CS, Nehrir MH, Shaw SR, 2005. Dynamic models and model validation for PEM fuel cells using electrical circuits. *IEEE Trans Energy Conv*, 20(2):442-451. <https://doi.org/10.1109/TEC.2004.842357>
- Wang Z, Luo M, Geng Y, et al., 2018. A model to compare convective and radiant heating systems for intermittent space heating. *Appl Energy*, 215:211-226. <https://doi.org/10.1016/j.apenergy.2018.01.088>
- Ward LC, Heitmann BL, 1998. Multiple frequency bioelectrical impedance analysis (MF BIA) and R-X plots in the assessment of obesity. Proc Aust Soc Study Obesity, 7:20.
- Ward LC, Heitmann BL, Craig P, et al., 2000. Association between ethnicity, body mass index, and bioelectrical impedance: implications for the population specificity of prediction equations. *Ann N Y Acad Sci*, 904(1):199-202. <https://doi.org/10.1111/j.1749-6632.2000.tb06449.x>
- Yousri DA, AbdelAty AM, Said LA, et al., 2017. Biological inspired optimization algorithms for cole-impedance parameters identification. *AEU-Int J Electron Commun*, 78:79-89. <https://doi.org/10.1016/j.aeue.2017.05.010>